REPORT DOCUMENTATION PAGE

AFRL-SR-AR-TR-03-

0424

1. AGENCY USE ONLY *(Leave blank)*	2. REPORT DATE	3. REPORT TYPE AND DATES COVERED
	8/25/03	Final 12/15/1999 - 05/31/2003

4. TITLE AND SUBTITLE

Fundamental Studies of Novel Contact-Damage Resistant Ceramics

5. FUNDING NUMBERS

Grant No. F49620-00-1-0104

6. AUTHOR(S)

Prof. Nitin P. Padture, University of Connecticut

Prof. Subra Suresh, Mass. Inst. of Technology

7. PERFORMING ORGANIZATION NAMES(S) AND ADDRESS(ES)

University of Connecticut
97 N. Eagleville Road
Storrs, CT 06269-3136

Mass. Inst. of Technology
77 Mass. Avenue
Cambridge, MA 02139

8. PERFORMING ORGANIZATION REPORT NUMBER

9. SPONSORING / MONITORING AGENCY NAMES(S) AND ADDRESS(ES)

AFOSR/NA
801 N. Randolph Street, Suite 732
Arlington, VA 22203-1977

10. SPONSORING / MONITORING AGENCY REPORT NUMBER

11. SUPPLEMENTARY NOTES

a. DISTRIBUTION / AVAILABILITY STATEMENT

Contact authors for additional copies

13. ABSTRACT *(Maximum 200 words)*

The concept of elastic-modulus-graded ceramics for improved resistance to quasi-static contact damage (Hertzian-indentation), sliding-contact damage, and wear was investigated. In these graded materials, the in-plane elastic modulus (E) is low at the contact surface and high in the interior (substrate) with a continuous, or step-wise continuous, E-gradation in-between. Processing strategies for fabricating such E-graded ceramic composites in the Al_2O_3-glass, the Si_3N_4-glass, and the Si_3N_4-SiC systems are described. The Hertzian indentation (quasi-static and sliding) behavior of these composites, along with some results from wear tests, are presented. Computational modeling (finite-element analysis or FEA) results are also presented, and are used to discuss the role of E-gradients in imparting contact-damage resistance to these materials. The use of calibrated FEA models as predictive tools for the design of next-generation graded materials is also discussed.

14. SUBJECT TERMS

DISTRIBUTION STATEMENT A
Approved for Public Release
Distribution Unlimited

15. NUMBER OF PAGES

19

16. PRICE CODE

17. SECURITY CLASSIFICATION OF REPORT	18. SECURITY CLASSIFICATION OF THIS PAGE	19. SECURITY CLASSIFICATION OF ABSTRACT	20. LIMITATION OF ABSTRACT
Unclassified	Unclassified	Unclassified	Unclassified

FUNDAMENTAL STUDIES OF NOVEL CONTACT-DAMAGE RESISTANT CERAMICS

AFOSR GRANT NUMBER F49620-~~96-1-0104~~ 00 -1-0104

Nitin P. Padture
Department of Metallurgy and Materials Engineering
University of Connecticut, Storrs, CT 06269-3136

Subra Suresh
Department of Materials Science and Engineering
Massachusetts Institute of Technology, Cambridge, MA 02139-4307

Abstract

The concept of elastic-modulus-graded ceramics for improved resistance to quasi-static contact damage (Hertzian-indentation), sliding-contact damage, and wear was investigated. In these graded materials, the in-plane elastic modulus (E) is low at the contact surface and high in the interior (substrate) with a continuous, or step-wise continuous, E-gradation in-between. Processing strategies for fabricating such E-graded ceramic composites in the Al_2O_3-glass, the Si_3N_4-glass, and the Si_3N_4-SiC systems are described. The Hertzian indentation (quasi-static and sliding) behavior of these composites, along with some results from wear tests, are presented. Computational modeling (finite-element analysis or FEA) results are also presented, and are used to discuss the role of E-gradients in imparting contact-damage resistance to these materials. The use of calibrated FEA models as predictive tools for the design of next-generation graded materials is also discussed.

1. Introduction and Background

Because of their innate hardness and stiffness, ceramics are routinely used in contact applications, where component surfaces are subjected to large stresses over highly localized contact areas (*e.g.* bearings, valves, nozzles, rollers, armor, wear-parts, microelectronic devices, dental implants, prostheses). This kind of contact-loading configuration, in the elastic limit, is typified by the Hertzian indentation test, which can also be used to gain fundamental information about the contact response of the material [1]. In this test, a punch or a sphere is used to deliver the contact load onto a test specimen, normal to the contact surface. Beyond a critical load, Hertzian cracks of the shape of a truncated cone (frustum) develop in the test ceramic. The tensile stresses generated by the indentation cause these cracks to initiate just outside the contact circle and propagate downwards and outwards into the material. These Hertzian cone cracks, which are extremely deleterious to strength and tribological performance, compromise the overall structural integrity of the ceramic component (see, for example, Refs. [1,2,3]).

Several approaches have been used to suppress the formation and propagation of Hertzian cone crack in ceramics. Most of them entail the introduction of a layer of compressive residual stresses at the surface using a variety of surface-modification techniques, such as tempering [1], layering [4], phase transformation [5], coating [6], ion-exchange [7], ion-implantation [8], differential densification [9], and grinding [10]. Other approaches are based on the introduction of heterogeneities within the microstructures of a ceramic [11, 12] or phase changes [13]. These heterogeneities can be in the form of elongated grains with weak grain boundaries or phase-

transforming particles which, under contact loading, suppress Hertzian cone cracks by creating a zone of distributed shear damage (inelasticity) beneath the indenter. Layering approaches based on this type of inelasticity have also been devised [14, 15, 16]. However, all these approaches have some drawbacks, including cracking along interfaces and susceptibility to mechanical fatigue [17, 18] and wear.

In this context, a new, fully-elastic approach for suppressing the formation of Hertzian cracks was invented by recourse to functionally-graded ceramics [19, 20, 21, 22, 23, 24, 25, 26, 27]. In this approach, the contact-surface region is elastic modulus (E) graded, such that the E is low at the contact surface and high in the interior. In such a E-graded ceramic, the principal tensile stresses that drive the cone cracks diffuse away from the surface, resulting in the suppression of the cracks.

The E-gradation approach is also useful in suppressing damage under sliding contacts, where a Hertzian sphere, under load, is translated normal to the loading direction at very low speeds. In the case of high-speed sliding wear conditions, where the contact loads used are typically very low, the E-gradation approach may be of limited applicability.

2. Theoretical Basis

Although there has been some theoretical work on the analysis of contact loading of graded structures in the geomechanics literature, the first comprehensive analysis pertaining to advanced materials was performed by Giannakopoulos and Suresh [26, 27]. An important finding of that study, relevant to the design of contact-damage-resistant elastic materials, is that certain types of E-gradations result in a beneficial redistribution of Hertzian tensile stresses in the material.

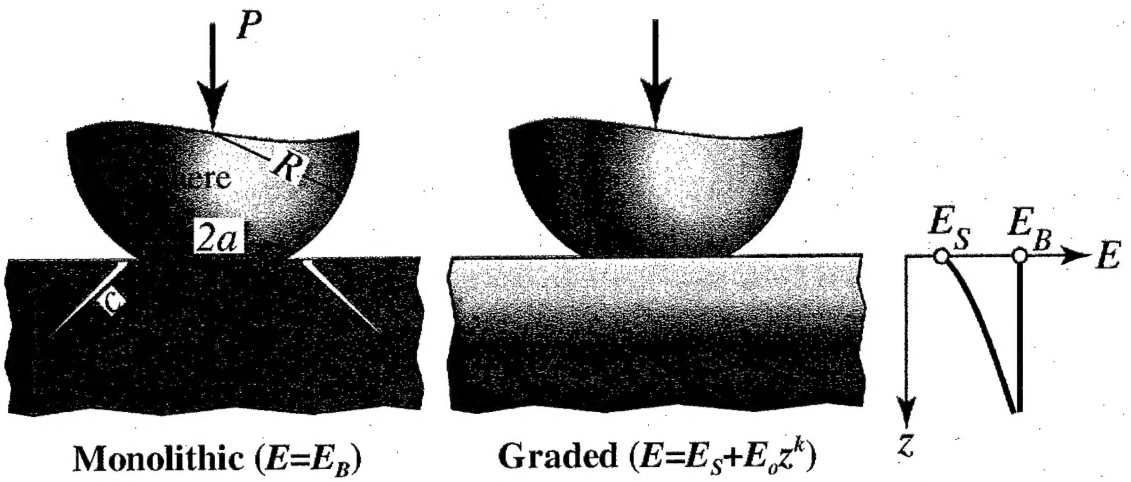

Fig. 1. Schematic diagram showing Hertzian indentation of monolithic ($E=E_B$) and E-graded ($E=E_S+E_oz^k$, approaching E_B) materials (cross-section views). Formation of the Hertzian cone-crack is depicted in the monolithic material. Schematic E-profiles are shown on the right.

Consider a monolithic material with a constant elastic modulus (E_B) and a material with E-gradation represented by a power-law function:

$$E=E_S+E_oz^k, \tag{1}$$

where E_S is the elastic modulus at the contact surface, E_o is a constant, z is the depth below the contact surface into the material, and k is a positive exponent (Figs. 1A and 1B). Under Hertzian

indentation (sphere of radius R), the monolithic material will develop a cone-crack when loaded beyond a critical contact load P^*. The cone crack nucleates at the surface and is driven by the Hertzian principal stress σ_1, which is tensile outside the contact circle and drops off rapidly with depth z [2]. The σ_1 scales with the indentation pressure p_o given by $P/\pi a^2$, where P is the contact load and a is the contact radius. In the E-graded material, the elastic modulus is low at the contact surface, and it increases with depth z. As a result, the principal stress σ_1 is redistributed relative to the monolithic case: by virtue of the higher E, σ_1 is higher in the interior of the material where it is least deleterious, and it is lower at the contact surface. This is somewhat analogous to fiber-reinforced composites, where majority of the applied stress is borne by the fibers by virtue of their higher E [28]. The net result of such stress redistribution is that, for a range of contact loads $P^*<P<P_{Max}$, the σ_1 is not sufficiently high to cause cone cracking in the E-graded material, whereas in the monolithic material, cone-cracking is expected under the same contact load. Note that cone-cracking is expected in the E-graded materials at sufficiently high contact loads $>P_{Max}$.

To experimentally corroborate these theoretical predictions and to explore other possible interesting contact-mechanical properties of E-graded materials, several sets of experiments and finite-element analyses (FEA) were conducted. In order to preclude complications associated with plastic deformation under contact loading in metals and polymers, these studies were limited to brittle, elastic ceramic systems.

3. Al_2O_3-Glass System

Fig. 2A shows the processing strategy for the fabrication of a E-graded Al_2O_3-glass composite. This method involves the impregnation of a dense, fine-grained Al_2O_3 of E=380 GPa by a low-elastic-modulus (E=70 GPa) alumino-silicate glass at elevated temperatures (1690 °C for 2 h in air), where the glass penetrates the Al_2O_3 grain boundaries [19, 29§]. The monolithic Al_2O_3 was sintered in-house using AKP-30 Al_2O_3 powder (Sumitomo Chemical, Japan) doped with 500 ppm MgO, and the glass was obtained commercially (Code 0317, Corning Inc., Corning, NY).

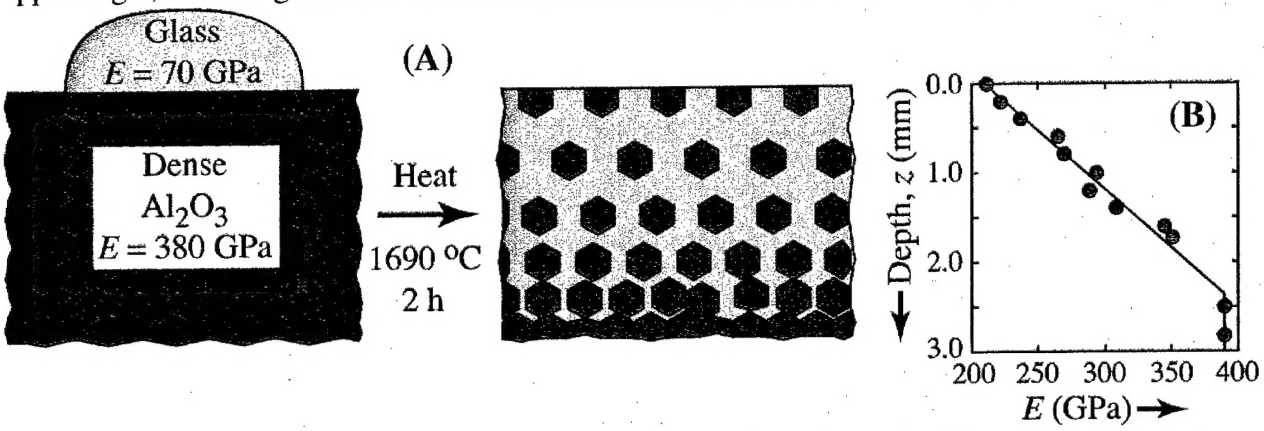

Fig. 2. (A) Schematic diagram showing the processing scheme for fabricating E-graded Al_2O_3-Glass composite (cross-section views). The glass and Al_2O_3 have the same Poisson's ratio and thermal expansion mismatch. (B) E-profile of the resulting E-graded Al_2O_3-Glass composite; straight line force-fitted to data. After Refs. [19, 29].

§ In order to eliminate closed porosity generated as a result of the glass impregnation process, hot-isostatic pressing was performed at 1500 °C at 100 MPa in N_2 atmosphere for 1 h [29].

Both the Al_2O_3 and the glass had the same Poisson's ratios (ν=0.22) and the same thermal expansion coefficients (α=8.8×10^{-6} °C^{-1}). Fig. 2B shows the *E*-profile of the resulting composite, as determined by cross-sectional image analysis in conjunction with a two-phase elastic model [30]. The amount of glass was found to vary from 42 vol% at the surface to 0 vol% in the interior over a depth of ~2.5 mm.

While monolithic glass and Al_2O_3 subjected to Hertzian (spherical) indentation tests resulted in classic cone cracks (Fig. 3A), under the same test conditions, cracking in the *E*-graded Al_2O_3-glass composite was suppressed completely (Fig. 3B). This is despite the fact that the *E*-graded Al_2O_3-glass composite has a lower toughness at the contact surface (2.3 MPa.m$^{0.5}$) relative to the monolithic Al_2O_3 (3.3 MPa.m$^{0.5}$). Also, there was no evidence of inelastic deformation.

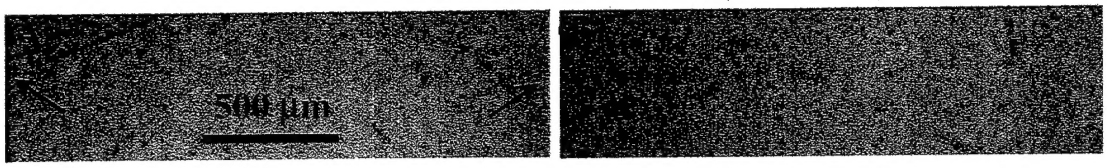

Fig. 3. Cross-sectional view (optical) of Hertzian indentation damage in: (A) monolithic Al_2O_3 and (B) *E*-graded Al_2O_3-glass (*P*=3000 N, WC-Co ball indenter *R*=4.76 mm). Arrows indicate tips of the cone-crack. After Ref. [29].

4. Finite Element Analysis (FEA)

FEA was used to determine the distribution of Hertzian principal stress σ_1 in monolithic and *E*-graded materials under the above experimental indentation condition. FEA was also used as a predictive tool to simulate stress fields for a range of hypothetical *E*-gradients, in an effort to provide guidelines for the design of *E*-graded material structures. The FEA was performed using a general purpose finite element package (ABAQUS Version 5.7, Hibbitt, Karlsson and Sorenson Inc., Providence, RI) [19]. Complete details of the numerical implementation of the indentation of graded materials are given in Refs. [26, 27, 31, 32]. The finite element mesh consisted of 4625 four-noded elements with 5058 nodes. An axisymmetric formulation was employed for the calculations. The spherical indenter was taken to be parabolic ($|z| = r^2/2R$, where r is the radial distance from the center of the contact circle), which is a good approximation for a sphere at normalized contact radii $a/2R < 0.2$. The absolute size of the mesh is also important. As such, the outer boundaries were designed to be at least 50 times the contact radius a. This ensures semi-infinite far field boundary conditions. Hertzian indentation was simulated on all bulk and graded materials studied, assuming purely elastic behavior. The input for FEA were the elastic properties of the indenter (*E*=614 GPa, ν=0.22) and the specimen materials. In the case of the monolithic material it was simply *E*=386 GPa, whereas for the *E*-graded materials a user subroutine was used to input the *E*-profile (*E*-*z* power-law function: $E=254+85z^{0.5}$; units of GPa and mm). This is a slightly different *E*-profile than the one shown in Fig. 2B and is for a different *E*-graded Al_2O_3-glass batch of materials. The in-plane elastic properties and the Poisson's ratio (ν= 0.22) for all materials were assumed to be the identical. It was also assumed that the indented materials were free of residual stresses.

An indentation load of P=3000 N and a ball radius R=4.76 mm (identical to the Hertzian indentation conditions used in the experiments) was applied in a single step. Extensive checking of the mesh resolution was performed by solving the spherical indentation problem for the monolithic material (constant elastic modulus); very good agreement (within 5%) was obtained between the results from FEA and analytical solutions [26, 27, 31, 32]. The accuracy of the FEA was also checked by comparing the values of the contact circle radii, a, resulting from the FEA and those measured experimentally, for both monolithic and graded materials. Once again, in each case the differences were found to be within 5%. Although the output from FEA is the full stress tensor, only values of the maximum principal tensile stresses at and just outside the contact circle are reported here.

Fig. 4 shows results from FEA, where the maximum tensile Hertzian stress σ_1 at the surface of the monolithic Al_2O_3 is 2.88 GPa (Fig. 4A), while that for the E-graded Al_2O_3-glass composite is 1.53 GPa (Fig. 4C) — a reduction of ~40% [19]. The maximum tensile stress for a composite of constant composition of Al_2O_3-42vol% Glass (non-graded) was found to be 1.84

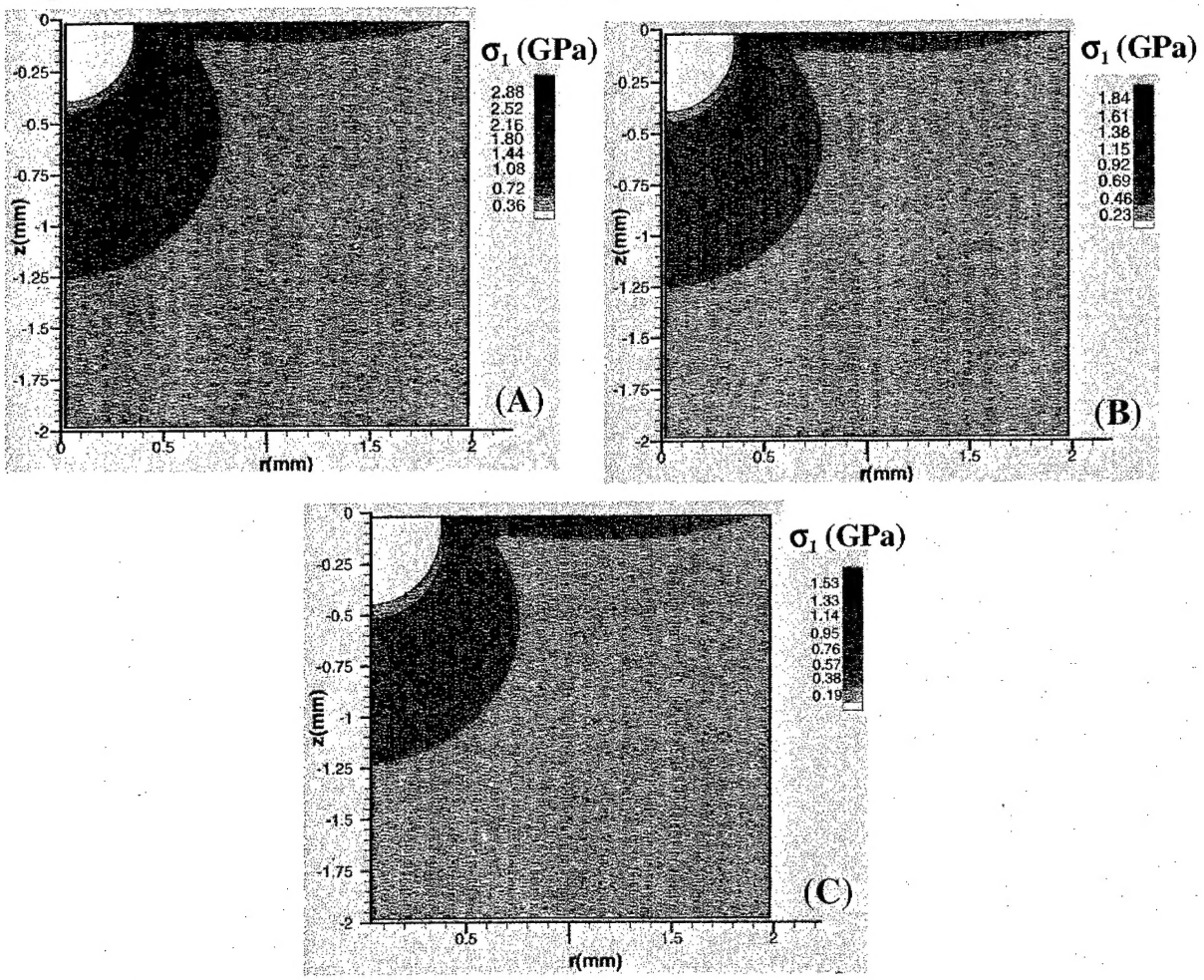

Fig. 4. FEA results for: (A) monolithic Al_2O_3, (B) Al_2O_3-42vol% Glass composite of fixed composition (non-graded), and (C) E-graded Al_2O_3-Glass composite. Cross-sectional views (one half) of iso-stress contours of the σ_1 Hertzian principal tensile stress. Hertzian indentation conditions identical to experiments (P=3000 N, WC-Co ball indenter R=4.76 mm). The blank region under the indenter is intense compression. After Ref. [19].

GPa (Fig. 4B). Since the thermal expansion coefficients of both the Al_2O_3 and the glass were matched, no residual stresses could be detected at the surface using two independent techniques: photo-luminescence piezo-spectroscopy and Vickers indentation. Thus, it was concluded that the suppression of Hertzian cone-cracking in the *E*-graded Al_2O_3-glass composite, despite its lower toughness, was solely due to the reduction of the maximum tensile Hertzian stress by virtue of the *E*-gradation [19].

5. Sliding Contact

Crack-suppression was also observed during slow-speed sliding of a Hertzian indenter (steel ball R=10 mm, E=280 GPa) across top contact surface of the *E*-graded Al_2O_3-glass composite (Fig. 5). Note the formation of "herring-bone" cracks in the monolithic Al_2O_3 at much lower loads (P=1600 N), whereas no cracks are seen in the *E*-graded case at P=2200 N [21]. In both cases the friction coefficient, μ, was measured to be 0.08.

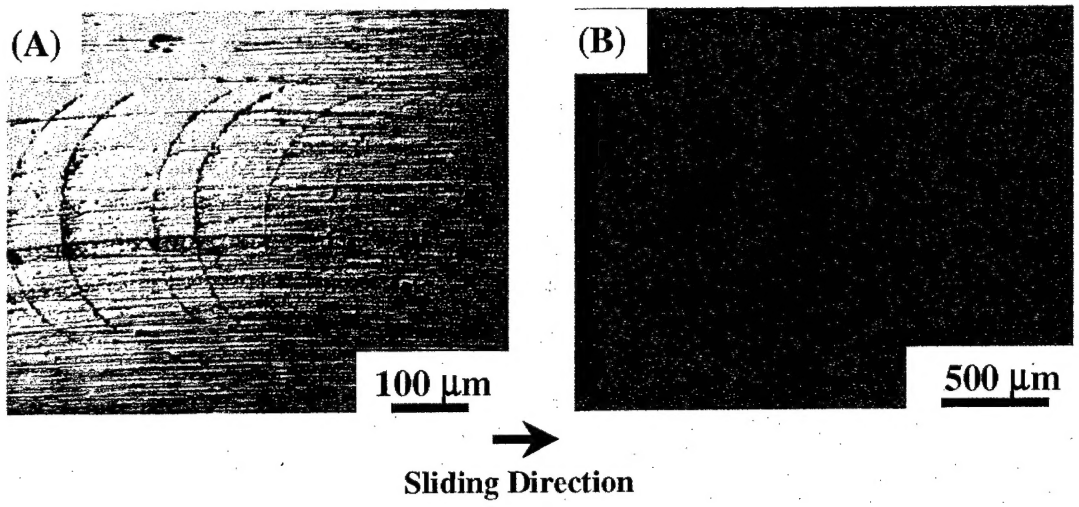

Fig. 5. Top view (optical) of sliding Hertzian indentation damage in: (A) monolithic Al_2O_3 (P=1600 N) and (B) *E*-graded Al_2O_3-Glass composite (P=2200 N). In both cases steel ball indenter R=10 mm was used, with a sliding velocity of 0.3 $mm.s^{-1}$. After Ref. [21].

The FEA analysis of frictional sliding contact requires a three-dimensional model. A method, which facilitates such three-dimensional analysis with appropriate modifications of the two-dimensional axisymmetric models, is the ring-element approach [21, 32]. The advantage of this approach is that it maps the entire three-dimensional field affected by indentation into a radial-axial plane of reference that includes the direction of sliding [21, 32]. This method, full details of which can be found in Ref. [32], requires less than $1/80^{th}$ of the computational time as compared to a full three-dimensional analysis for the particular problem considered here [21].

In the simulations, first the normal load was applied monotonically until it reached the peak load P used in the experiments. Then the tangential load Q was gradually increased up to its maximum value μP, while the normal load P was held constant. The input for FEA were the elastic properties of the steel indenter (E =280 GPa, ν=0.3) and the specimen materials, given in the section above. Similar to the FEA of Hertzian indentation, the accuracy of the FEA of sliding contact was checked by comparing the values of the contact circle radii, a, resulting from

the FEA and those measured experimentally, for both monolithic and graded materials. Once again, in each case the differences were found to be within 5%. The FEA results for sliding contact are shown in Fig. 6, where the maximum principal tensile stress (σ_1) at the trailing contact edge is found to be 1.2 GPa for the monolithic case, as compared with 0.9 GPa for the *E*-graded case. The reduced maximum tensile stress at the surface in the *E*-graded material is deemed responsible for the suppression of the "herring bone" cracks in that material.

Cracking associated with non-static contacts controls other related properties such as erosion and impact resistance. Therefore, the *E*-gradation approach which is used to suppress

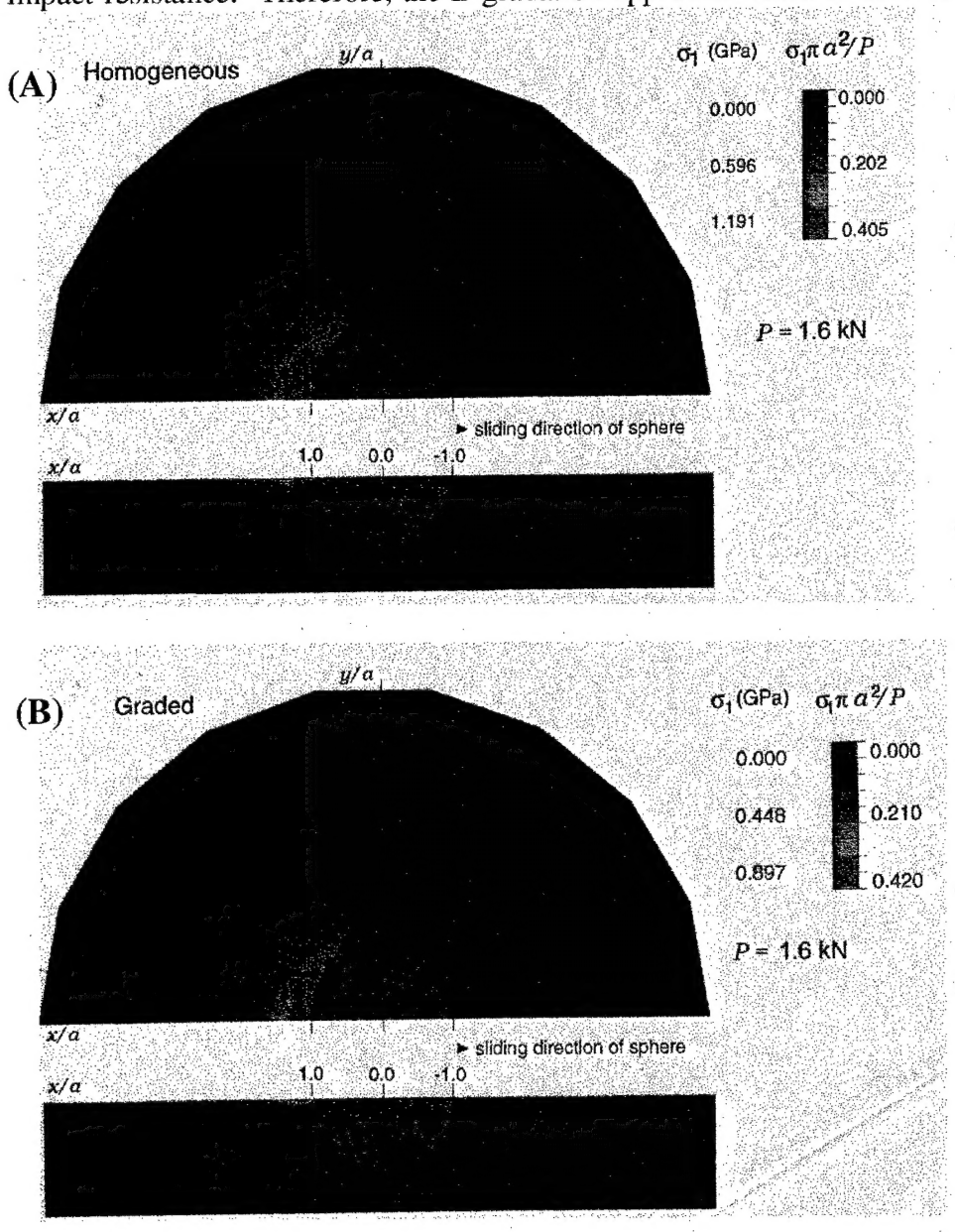

Fig. 6. Results from FEA showing iso-stress (σ_1) contours for the sliding Hertzian indentation of: (A) monolithic Al_2O_3 and (B) *E*-graded Al_2O_3-Glass composite (*P*=1600 N, steel ball indenter *R*=10 mm). Top figures in both (A) and (B) are half top-views and bottom figures are full cross-section views. After Ref. [21].

contact-induced cracking is also likely to be useful in enhancing the resistance of ceramics subjected to erosion and impact. This has been demonstrated to be the case in the *E*-graded Al_2O_3-glass composites, where significant improvements in erosion resistance [33] and impact resistance [34].

6. Si_3N_4-Glass System

Due to its combination of high toughness and hardness, Si_3N_4 is the ceramic of choice for contact applications (*e.g.* bearings, wear-parts, valves, seals). In order to demonstrate the use of the above *E*-gradation concept for improving the contact-damage resistance in Si_3N_4, the same processing strategy depicted in Fig. 2A was used to process *E*-graded Si_3N_4-glass composites [22]. In this case, dense, fine-grained Si_3N_4 (E=310 GPa) was impregnated by an oxynitride glass (E=110 GPa) at 1500 °C for 2 h in argon atmosphere; both the monolithic Si_3N_4 and the oxynitride glass were prepared in-house. Post-processing hot-isopressing was not necessary in the this case. The Si_3N_4 and the oxynitride glass had the same Poisson's ratios (ν=0.22) and the same thermal expansion coefficients (~3.5×10^{-6} °C^{-1}). Figs. 7A to 7C show cross-sectional microstructures taken using a scanning electron microscope (SEM) of the *E*-graded Si_3N_4-glass composite (chemically-etched using hydrofluoric acid) at 3 different glass-impregnation depths [22]. Note the decreasing amount of glass with increasing depth, as delineated by HF-etching, which has etched the glass away. The corresponding *E*-profile is plotted in Fig. 8, showing a ~38% increase in *E* over a depth of ~400 μm. The *E*-profile was measured using two methods, image analysis in conjunction with the two-phase model and quantitative nanoindentation, showing excellent agreement. The amount of glass was found to vary from 31 vol% at the surface to 0 vol% in the interior over a depth of 400 μm. The surface toughness of the monolithic Si_3N_4 and the graded Si_3N_4-glass composite was found to be 4.5 MPa.$m^{0.5}$ and 2.3 MPa.$m^{0.5}$, respectively [22].

Fig. 9A shows Hertzian cone-cracks produced in monolithic Si_3N_4, while no cracks are seen in the graded Si_3N_4-glass composite (Fig. 9B) under identical indentation conditions [22]. The FEA, using the method described in section 4, results in Figs. 10A and 10B show that the maximum tensile Hertzian stress at the surface of the monolithic Si_3N_4 is 2.56 GPa, while that for the graded Si_3N_4-glass composite is 1.76 GPa, a reduction of ~30% [22]. Note that an *E*-profile of the type $E=250+300z^{0.65}$ (units of GPa and mm) was used, which is slightly different from the one observed in Fig. 8. Since the thermal expansion coefficients of both the Si_3N_4 and the glass were matched, no residual stresses are expected. This once again demonstrates that, by virtue of the *E*-gradation alone, the principal tensile Hertzian stresses that drive the cone cracks diffuse away from the surface into the interior where they are less deleterious.

Although the experimental studies were limited to one particular *E*-graded material in this system with a certain *E*-profile, the calibrated FEA can now be used as a predictive tool to simulate stress fields for a range of hypothetical *E*-gradients, in an effort to provide guidelines for the design of *E*-graded material structures. To that end, four different types of hypothetical *E*-profiles (see Eqn. 1) were considered, and are plotted in Fig. 11 [22]. The Hertzian indentation responses for these *E*-profiles were then computationally simulated, and the corresponding maximum principal tensile stress σ_1, which is responsible for the Hertzian cone cracks, was computed. The FEA Hertzian indentation conditions were the same as those used in the experiments. The reductions in the maximum tensile stress for the graded surfaces relative to the monolithic Si_3N_4 case, are also given in Fig. 11.

Fig. 7. SEM micrographs of chemically (HF)-etched Si_3N_4-glass graded material at 3 different glass-impregnation depths: (A) $z = 0$ (surface), (B) $z = 0.1$ mm, and (C) $z = 0.5$ mm (bulk). Note that the glass has been etched away by the hydrofluoric acid. After Ref. [22].

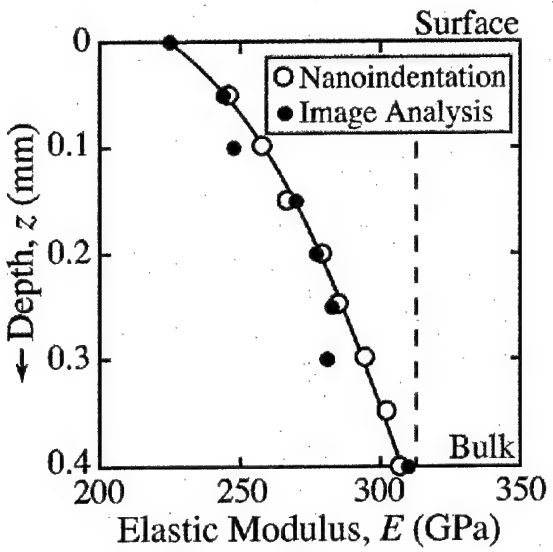

Fig. 8. Elastic modulus profile of the *E*-graded Si_3N_4-glass; glass impregnated at 1500°C for 2 h. The elastic modulus (E) at a given depth (z) was estimated using two different methods: (i) quantitative image analysis in conjunction with a two-phase model (solid symbols) [22] and (ii) quantitative nanoindentation (open symbols).

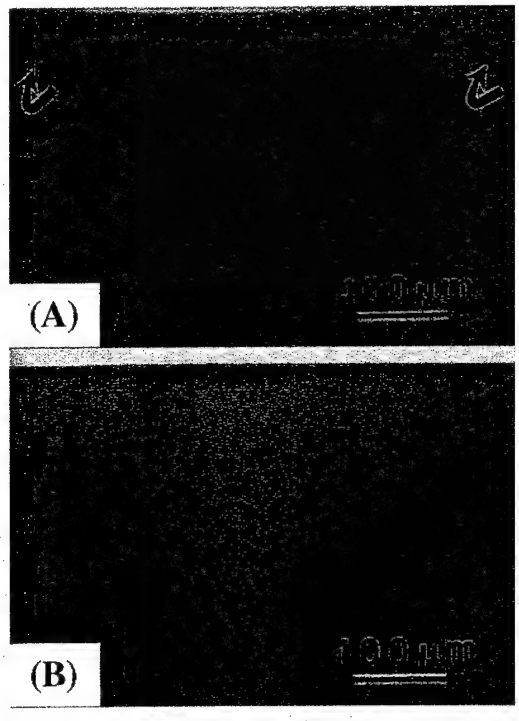

Fig. 9. Optical micrographs showing cross-sectional views of Hertzian indentation damage in: (A) monolithic Si_3N_4 and (B) *E*-graded Si_3N_4-glass. Hertzian indentation performed under identical conditions: P=3000 N, WC-Co ball indenter R=4.76 mm. After Ref. [22].

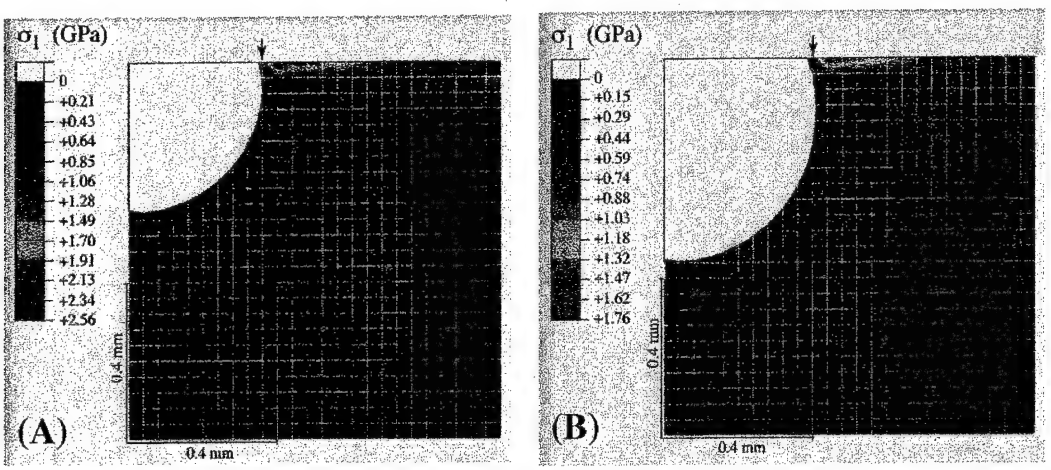

Fig. 10. FEA results for: (A) monolithic Si_3N_4 and (B) *E*-graded Si_3N_4-glass. Cross-sectional views (one half) of iso-stress contours of the σ_1 Hertzian principal tensile stresses. Hertzian indentation conditions identical to experiments (*P*=3000 N, *R*=4.76 mm). The blank region under the indenter is intense compression. Arrow indicates edge of the contact. After Ref. [22].

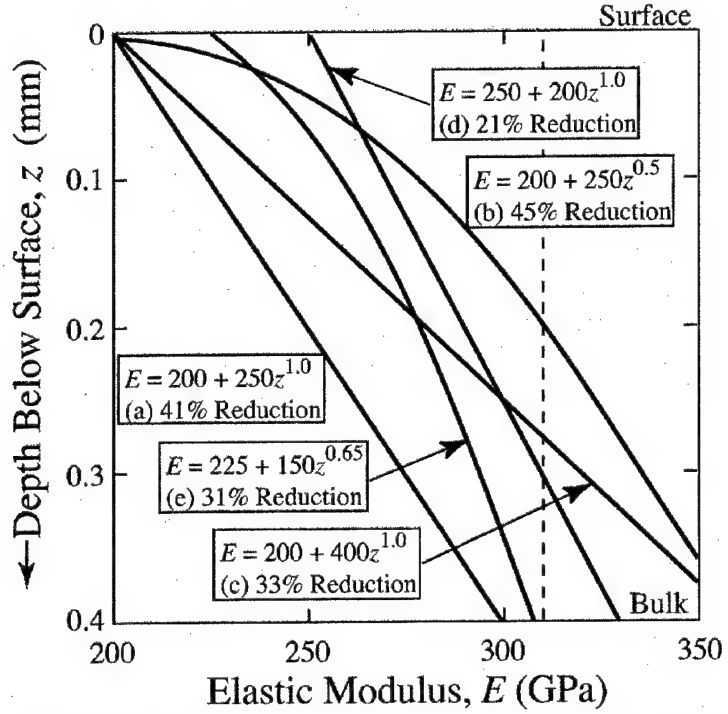

Fig. 11. Hypothetical *E*-profiles (a to d) and the corresponding % reduction in the σ_1 Hertzian principal tensile stresses computed from FEA. *E*-profile (e) represents the Si_3N_4-glass *E*-graded material (Fig. 10). The vertical dashed line represents monolithic Si_3N_4 elastic modulus. After Ref. [22].

First consider the effect of E-profile shape: curves (a) linear or (b) parabolic, with the same E_S=200 GPa and E_o=250 GPa, in Fig. 11. The % reduction is somewhat greater (45%) for the parabolic E-profile as compared to the linear E-profile (41%). A more rapid change in E in the near-surface region — a region where the tensile stresses drop-off rapidly with depth (Fig. 10) — results in a greater decrease in the maximum tensile stress. However, at a given depth near the surface the absolute E is higher for the parabolic E-profile case, which results in an increase in the maximum tensile stress. These countervailing effects rationalize the small differences in the relative reductions in the two cases. This notion is further reinforced by considering another linear E-profile (curve (c)) in Fig. 11. Although curve (c) is steeper relative to curve (a), the absolute value of the elastic modulus, E , is relatively higher at a given depth near the surface. The latter effect is more pronounced here, resulting in only a 33% reduction in the maximum tensile stress. Finally, the effect of E_S is shown in curve (d): a higher E at the surface results in a significantly lower % reduction in the maximum tensile stress. Thus, in order to achieve a significant decrease in the maximum tensile stress in a graded material under Hertzian indentation relative to its monolithic counterpart, the following two design guidelines emerge: (i) a large difference between E_S and E_B and (ii) a rapid decrease in E near the surface (exponent $k < 1$, preferably < 0.5) [22].

7. Si_3N_4-SiC System

Although Hertzian cone-cracks in these E-graded Al_2O_3-glass and Si_3N_4-glass materials are suppressed, the contact surfaces of these materials contain 30 to 40 vol% glass, rendering them brittle and prone to wear degradation [25, 35]. Fig. 12 compares the wear properties of the various Si_3N_4-based materials [25]. For the Si_3N_4-glass graded material the wear transition from plasticity-controlled mild wear to fracture-controlled severe wear occurs at ~8 min (Fig. 12A), whereas that for monolithic bulk Si_3N_4 occurs at ~150 min (Fig. 12B). To that end, stepwise-graded composites in the Si_3N_4-SiC system were fabricated using pressureless co-sintering, where the lower elastic modulus Si_3N_4 (E=310 GPa) forms the tough, wear-resistant contact surface and the higher elastic modulus SiC (E=390 GPa) forms the substrate [23, 25]. Here fine starting powders (<0.5 μm) of both Si_3N_4 (SN-E10, Ube Industries, Japan) and SiC (UF-15, H.C. Stark, Germany), but a gradient in the amount of yttrium aluminum garnet (YAG) sintering additive to match the sintering rates of the Si_3N_4 and SiC end members: 2 vol% YAG + 98 vol% Si_3N_4 at the contact surface, grading to 20 vol% YAG + 80 vol% SiC in the substrate. The stepwise-graded composite (Fig. 13) was created by laying down 9 powder layers of different compositions and compacting them, followed by sintering under 0.1 MPa N_2 overpressure at 1900 °C for 1 h in a hot-isostatic press. Although the overpressure does not assist in the sintering, it ensures the stability of both Si_3N_4 and SiC in contact with each other at the sintering temperature [23, 25, 36]. The contact-surface of this composite had a fine-grained Si_3N_4 (~3 μm), 2 vol% YAG additive, and low porosity (3-5%).

Fig. 14 shows the suppression of Hertzian cone-cracks in this stepwise-graded Si_3N_4-SiC composite; cone-cracks are observed in monolithic Si_3N_4 and SiC end members under identical indentation condition (not shown here). It is believed that a combination of two factors primarily contribute to this cone-crack suppression: (i) reduction in the maximum tensile Hertzian stress at the surface by virtue of the E-gradient and (ii) thermal-expansion-mismatch residual compressive stresses at the contact surface [25]. Note that inelastic damage can also contribute to the crack suppression [11, 12], but considering the small extent of the damage (Fig. 14), this mechanism is

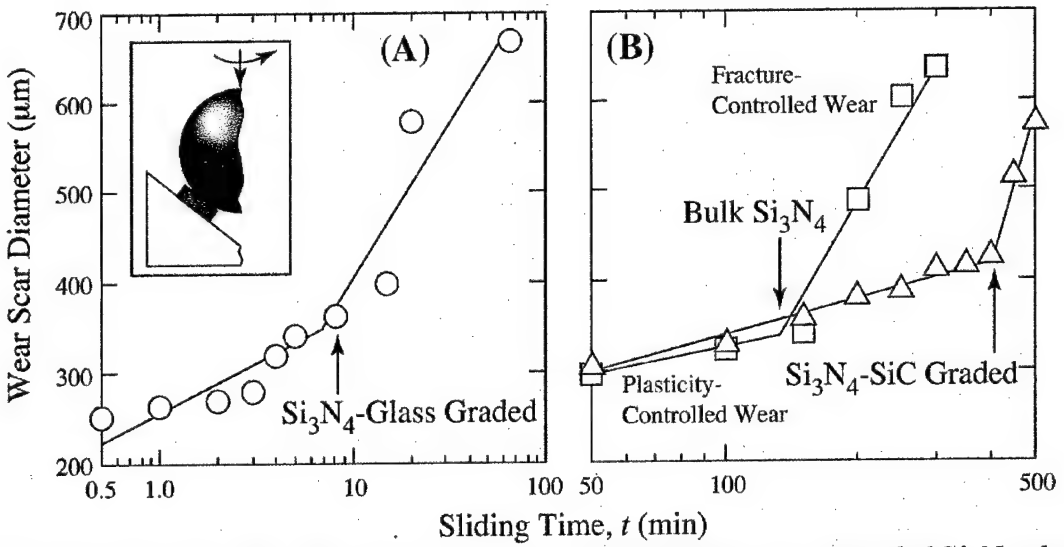

Fig. 12. Wear scar diameter as a function of sliding time for: (A) *E*-graded Si_3N_4-glass and (B) monolithic Si_3N_4 and Si_3N_4-SiC graded composite. Data is plotted on two different graphs for clarity. Each datum point represents average of 3 specimens per material. Error bars are comparable to symbol size. Arrows indicate onset of transition between plasticity- and fracture-controlled wear. Inset is a schematic diagram showing one-half cross-sectional view of the testing geometry; shaded rectangle represents disk specimen (3.18 mm radius, 2.5 mm thick) and the ball (Si_3N_4) radius is 6.35 mm. The rotation speed is 100 rpm (0.04 $m.s^{-1}$ surface velocity) and the contact load is 80 N, under fully lubricated conditions. After Ref. [25].

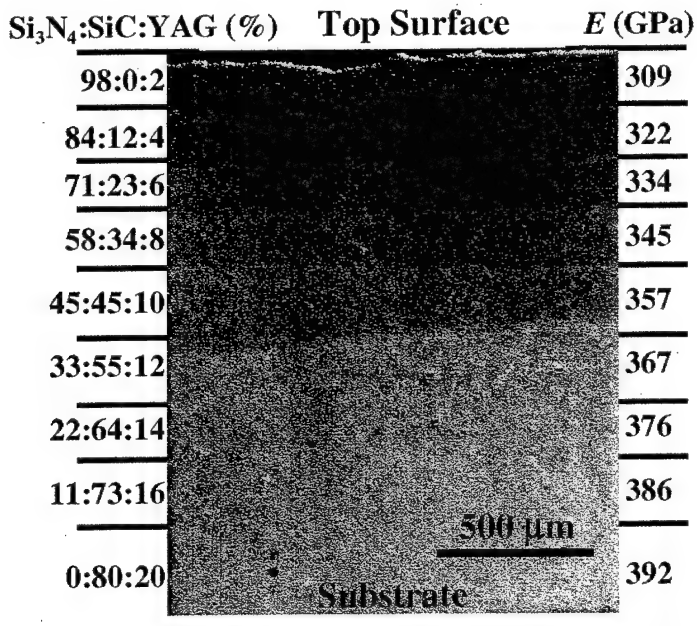

Fig. 13. Cross-sectional optical micrograph of the 9-layer Si_3N_4-SiC graded composite. The phase compositions (vol%) and the elastic moduli of the individual layers are given to the left and the right of the micrograph, respectively. After Ref. [25].

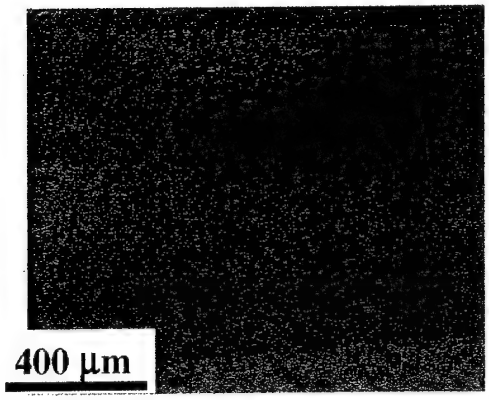

Fig. 14. Optical micrograph showing cross-sectional view of the Hertzian indentation damage in the 9-layer, step-wise graded Si_3N_4-SiC graded composite (P=3500 N, WC-Co ball indenter R=3.16 mm). Note the lack of cone-cracking, presence of small amount of inelastic damage, and faint outlines of the interlayer boundaries. After Ref. [25].

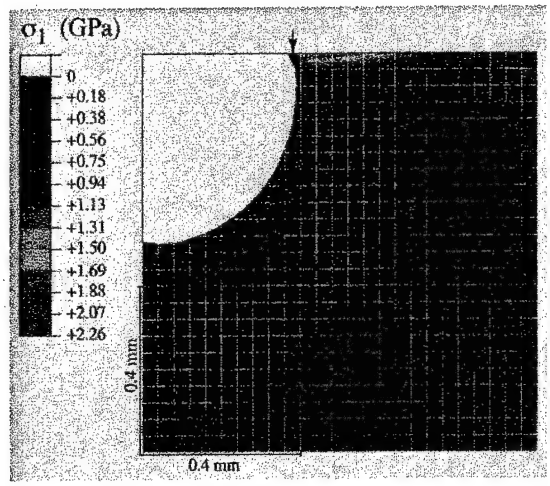

Fig. 15. FEA results for a step-wise graded Si_3N_4-SiC composite. Cross-sectional views (one half) of iso-stress contours of the σ_1 Hertzian principal tensile stresses (P=3000 N, R=4.76 mm). The blank region under the indenter is intense compression. Arrow indicates edge of the contact. After Ref. [23].

likely to be less important here. With regards to the E-gradient, FEA (using the method described in section 4) results show that the maximum tensile Hertzian stress at the surface of the monolithic Si_3N_4 is 2.56 GPa (Fig. 10A), while that for the stepwise-graded Si_3N_4-SiC composite (with a slightly different E-profile that the one shown in Fig. 13) is 2.26 GPa (Fig. 15), a reduction of modest 12% [23]. With regards to residual stresses, there is a moderate thermal-expansion mismatch between the Si_3N_4 and SiC end members ($\Delta\alpha$=1.5×10^{-6} °C^{-1}) in this E-graded material, which can induce compressive residual stresses ($\sigma_R \sim \Delta\alpha E \Delta T$) at the center of the contact surface, of the order of 800 MPa for average E~350 GPa and ΔT~1500 °C. This magnitude of σ_R was independently confirmed using the Vickers indentation test [25].

In addition to the cone-crack suppression, this E-graded composite possesses wear properties that are significantly improved over monolithic Si_3N_4 and graded Si_3N_4-glass composite, where the wear transition occurs at ~400 min (Fig. 12B) [25]. The improved wear resistance, as manifest by the delay of the transition from plasticity- to fracture-controlled wear, is attributed to the compressive stress (σ_R) present at the Si_3N_4 contact surface. Note that the small loads used in the wear test (P=80 N, Si_3N_4 ball radius R=6.35 mm) limits the active contact stress field to the first layer (~150 μm). In other words, for the wear test, the length scale of the E-gradient is much greater than the length scale of the contact stress field. A modification of the wear model by Lawn and co-workers [37] has been successfully used to rationalize the wear results, which provides a framework for the analysis of wear data, not only in terms of microstructural variables but also in terms of other important variables such as residual stresses [25]. These results show that the introduction of surface compressive residual stresses, which have been used in the past to increase the strength and apparent toughness of ceramics, can significantly improve the wear resistance of polycrystalline ceramics. This has important implications for the design of contact-damage-resistant ceramics.

8. Concluding Remarks

Ceramics are being increasingly used in contact application, where length scales involved can range from nanometers to millimeters. Steep stress-gradients over these length scales are ubiquitous in contact loading. In this context, we have demonstrated unequivocally that the E-gradient approach can be used to alleviate the intensities of the stress gradients and to improve the contact-damage resistance of ceramics. This approach relies on elasticity and is also very versatile, making it attractive for use in many applications involving repeat loading: *e.g.* bearings, valves, nozzles, rollers, wear-parts, microelectronics, data storage devices, dental implants, prostheses, MEMS, tooling for manufacturing. Our understanding of contact-mechanics of E-graded materials and its computational modeling has advanced to the extent that we can now perform predictive modeling, and provide design guidelines for E-graded materials. Processing of materials to achieve these E-gradients suitable for the appropriate applications is perhaps the most challenging task ahead. Although the processing strategies will be highly dependent on the specific material systems and geometries, there are several processing methods available at our disposal: vapor-phase deposition; solution routes to deposition; thermal spray; hydrothermal deposition; differential sintering; impregnation of porous or dense pre-forms; diffusion.

Acknowledgements

This work was sponsored (in part) by the Air Force Office of Scientific Research, under Grant# F49620-96-1-0104. The contributions of the following are gratefully acknowledged: Dr. M. Dao, Dr. A.E. Giannakopoulos, Dr. J. Jitcharoen, Ms. A. Pandit, Dr. D.C. Pender, and Mr. S.C. Thompson. The views and conclusions contained herein are those of the authors and should not be interpreted as necessarily representing the official policies or endorsements, either expressed or implied, of the Air Force Office of Scientific Research or the U.S. Government.

References

1. B. R. Lawn, *Fracture of Brittle Solids — Second Edition* (Cambridge University Press, Cambridge, U.K., 1993).
2. B. R. Lawn, *Journal of the American Ceramic Society* 81, 1977 (1998).
3. N. P. Padture, in *Encyclopedia of Materials: Science and Technology*, ed. R.W. Cahn, K.H.J. Buschow, M.C. Flemings, B. Ilschner, E. Kramer and S. Mahajan (Pergamon Press, New York, NY, 2001) p. 3750
4. R. Satyamoorthy, A. V. Virkar and R. A. Cutler, *Journal of the American Ceramic Society* 75, 1136 (1992).
5. D. J. Green, R. H. J. Hannink and M. V. Swain, *Transformation Toughening of Ceramics* (CRC Press, Boca Raton, FL, 1989).
6. S. Bull and P. R. Chalker, *Journal of Metals* 47, 16 (1995).
7. R. Tandon and D. J. Green, *Journal of the American Ceramic Society* 74, 1981 (1991).
8. C. W. White, C. J. McHargue, P. S. Skald, L. A. Boatner and G. C. Farlow, *Materials Science Reports* 4, 41 (1989).
9. K. Chyung, in Nucleation and Crystallization in Glasses, *Advances in Ceramics*, ed. J. H. Simmons, D. R. Uhlmann and G. H. Beall (The American Ceramic Society, Columbus, OH, USA, 1982) p. 341.
10. H. P. Kirchner, *Strengthening of Ceramics* (Marcel Dekker, New York, NY, USA, 1979).
11. N. P. Padture and B. R. Lawn, *Journal of the American Ceramic Society* 77, 2518 (1994).
12. B. R. Lawn, N. P. Padture, H. Cai and F. Guiberteau, *Science* 263, 1114 (1994).
13. A. Pajares, F. Guiberteau, B. R. Lawn and S. Lathabai, *Journal of the American Ceramic Society* 78, 1083 (1995).
14. L. An, H. M. Chan, N. P. Padture and B. R. Lawn, *Journal of Materials Research* 11, 204 (1996).
15. D. C. Pender and N. P. Padture, *Journal of Materials Science Letters* 17, 999 (1998).
16. H. M. Chan, *Annual Reviews of Materials Science* 27, 249 (1997).
17. F. Guiberteau, N. P. Padture, H. Cai and B. R. Lawn, *Philosophical Magazine* A68, 1003 (1993).
18. N. P. Padture and B. R. Lawn, *Acta Metallurgica et Materialia* 43, 1609 (1995).
19. J. Jitcharoen, N. P. Padture, A. E. Giannakopoulos and S. Suresh, *Journal of the American Ceramic Society* 81, 2301 (1998).
20. S. Suresh and A. Mortensen, *Fundamentals of Functionally Graded Materials* (IOM Communications Ltd., London, UK, 1998).
21. S. Suresh, M. Olsson, A. E. Giannakopulos, N. P. Padture and J. Jitcharoen, *Acta Materialia* 47, 3915 (1999).
22. D. C. Pender, N. P. Padture, A. E. Giannakopoulos and S. Suresh, *Acta Materialia* 49, 3255 (2001).

23. D. C. Pender, S. C. Thompson, N. P. Padture, A. E. Giannakopoulos and S. Suresh, *Acta Materialia* 49, 3263 (2001).
24. S. Suresh, *Science* 292, 2447 (2001).
25. S. C. Thompson, A. Pandit, N. P. Padture and S. Suresh, *Journal of the American Ceramic Society* 85, (2002).
26. A. E. Giannakopoulos and S. Suresh, *International Journal of Solids and Structures* 34, 2357 (1997).
27. A. E. Giannakopoulos and S. Suresh, *International Journal of Solids and Structures* 34, 2393 (1997).
28. D. Hull and T. W. Clyne, *An Introduction to Composite Materials* (Cambridge University Press, Cambridge, UK, 1996).
29. J. Jitcharoen, Ph.D. Thesis, University of Connecticut, Storrs, CT, 1999.
30. Z. Hashin and S. Shtrikman, *Journal of the Mechanics and Physics of Solids* 11, 127 (1963).
31. S. Suresh, A. E. Giannakopoulos and J. Alcala, *Acta Materialia* 45, 1307 (1997).
32. A. E. Giannakopoulos and S. Suresh, *Acta Materialia* 46, 177 (1998).
33. R.P. Panat, K. Jakus, J.E. Ritter and P. Shah, *Ceramic Engineering and Science Proceedings* 21, 635 (2000).
34. P. Shah, K. Jakus and J.E. Ritter, in Functionally Graded Materials 2000, *Ceramics Transactions*, ed. K. Trumble, K. Bowman, I. Reimanis and S. Sampath (The American Ceramic Society, Westerville, OH, USA, 2001) p. 651.
35. D. C. Pender, Ph.D., University of Connecticut, Storrs, CT, 1999.
36. K. G. Nickel, M. J. Hoffmann, P. Greil and G. Petzow, *Advanced Ceramic Materials* 3, 557 (1988).
37. S.-J. Cho, B. J. Hockey, B. R. Lawn and S. J. Bennison, *Journal of the American Ceramic Society* 72, 1249 (1989).

Personnel Supported

University of Connecticut

Dr. Nitin Padture	Professor and Interim Department Head
Mr. Scott Thompson	Graduate Student, M.S. (graduated in September 2001; now employed by Carpenter Advanced Ceramics, Auburn, CA)
Ms. Anjali Pandit	Graduate Student, M.S. (graduated in May 2002; now employed by Shipley, Corp., Marlborough, MA)
Mr. Xiaoping Wang	Graduate Student, Ph.D.
Mrs. Xiaotong Wang	Graduate Student, M.S.

Massachusetts Institute of Technology

Dr. Subra Suresh	Ford Foundation Professor and Department Head
Dr. Antonios Giannakopoulos	Research Associate
Dr. Ming Dao	Research Associate
Mr. Nuwong Chollakoop	Graduate Student, Ph.D.

Publications

1. D.C. Pender, N.P. Padture, A.E. Giannakopoulos and S. Suresh, "Gradients in Elastic Modulus for Improved Contact-Damage Resistance: Part I, The Silicon Nitride-Oxynitride Glass System," ***Acta Materialia***, **49**, 3255-62 (2001).
2. D.C. Pender S.C. Thompson, N.P. Padture, A.E. Giannakopoulos and S. Suresh, "Gradients in Elastic Modulus for Improved Contact-Damage Resistance: Part II, The Silicon Nitride-Silicon Carbide System," ***Acta Materialia***, **49**, 3263-68 (2001).
3. S. Suresh, "Graded Materials for Resistance to Contact Deformation and Damage," *Science*, 292 [5526] 2447-51 (2001).
4. S.C. Thompson, A. Pandit, N.P. Padture and S. Suresh, "Stepwise-Graded Si_3N_4-SiC Ceramics with Improved Wear Properties," ***Journal of the American Ceramic Society***, **85** [8] 2059-64 (2002).
5. A. Pandit and N.P. Padture, "Interfacial Toughness of Diamond-Like Nanocomposite Thin Films on Ceramic Substrates," ***Journal of Materials Science Letters***, in press (2003).
6. N.P. Padture, "Graded Ceramics for Improved Contact-Damage Resistance," ***Materials Science Forum***, **423-425**, 125-130 (2003).

7. N.P. Padture, "Graded Ceramics for Improved Contact-Damage Resistance: A Review," ***International Journal of Computational Engineering and Science***, in press (2003).

Major Awards Received

S. Suresh: Distinguished Scientist/Engineering, TMS, February 2001
S. Suresh: Kelly Lecture, Cambridge University, UK, June 2001
S. Suresh: Elected to the National Academy of Engineering, February 2002
S. Suresh: R. B. Trull Distinguished Lecture, The University of Texas at Austin, March 2002

Transitions

S. Suresh, A.E. Giannakopoulos, N.P. Padture and J. Jitcharoen, "Functionally-Graded Materials," ***European Patent***, **No. 0968153** (2002).

S. Suresh, A.E. Giannakopoulos, N.P. Padture and J. Jitcharoen, "Method and Apparatus for Determination of Mechanical Properties of Functionally Graded Materials," ***United States Patent,*** pending.

S. Suresh, A.E. Giannakopoulos, R. Thampuran, O. Jorgensen, N.P. Padture and J. Jitcharoen, "Functionally Graded Materials and Engineering of Tribological Resistance at Surfaces," ***United States and European Patents,*** pending.